1-1-2003

Proper Orthogonal Decomposition Based Modeling and Experimental Implementation of a Neurocontroller for a Heat Diffusion System

Prashant Prabhat

S. N. Balakrishnan
Missouri University of Science and Technology, bala@mst.edu

Dwight C. Look
Missouri University of Science and Technology

Radhakant Padhi

Recommended Citation

P. Prabhat et al., "Proper Orthogonal Decomposition Based Modeling and Experimental Implementation of a Neurocontroller for a Heat Diffusion System," *Proceedings of the 2003 American Control Conference, 2003*, Institute of Electrical and Electronics Engineers (IEEE), Jan 2003.
The definitive version is available at https://doi.org/10.1109/ACC.2003.1243478

Proper Orthogonal Decomposition Based Modeling and Experimental Implementation of a Neurocontroller for a Heat Diffusion System

P. Prabhat, S. N. Balakrishnan[1], D. C. Look Jr., R. Padhi

Dept. of Mechanical and Aerospace Eng. and Engineering Mechanics

University of Missouri-Rolla, MO, 65409, USA

Abstract

Experimental implementation of a dual neural network based optimal controller for a heat diffusion system is presented. Using the technique of Proper Orthogonal Decomposition (POD), a set of problem-oriented basis functions are designed taking the help of experimental data as snap shot solutions. Using these basis functions in Galerkin projection, a reduced-order analogous lumped parameter model of the distributed parameter system is developed. This model is then used in an analogous lumped parameter problem. A dual neural network structure called *adaptive critics* is used to obtain optimal neurocontrollers for this system. In this structure, one set of neural networks captures the relationship between the states and the control, whereas the other set captures the relationship between the states and the costates. The lumped parameter control is then mapped back to the spatial dimension, using the same basis functions, to result in a feedback control. The controllers are implemented at discrete actuator locations. Modeling aspects of the heat diffusion system from experimental data are discussed. Experimental results to reach desired final temperature profiles are presented.

1. Introduction

Distributed Parameter Systems (DPS) arise in various application areas such as thermal processes, vibrating structures, fluid flow systems and so on. The control of DPS, which are governed by a set of Partial Differential Equations (PDEs), is an active field of research.

Because of their inherent nature, DPS problems have infinite number of modes and hence are otherwise known as infinite dimensional systems. Since it is impossible to deal with an infinite problem taking into account all of its modes, there is a need for developing approximate finite-dimensional models (preferably of small order) which should describe the system as accurately as possible. One techniques of a low-order finite-dimensional model development is Proper Orthogonal Decomposition (POD), followed by Galerkin projection [Ravindran]. In this approach, a set of problem-oriented orthogonal basis functions is first designed to approximately span the solution space of the original system. It is done through the so-called "snap-shot solutions", which by definition are supposed to be the representative solutions of the system at arbitrary instants of time. These basis functions, when used in the Galerkin projection scheme, lead to a low-order finite-dimensional approximate model of the system. This low-order model can then be used for control design using the known techniques for finite-dimensional systems.

In this paper, we first present an overview of the experimental setup, which represents a one-dimensional heat diffusion system with insulated boundary conditions. Then we discuss the use of experimental data to design the basis functions. The system parameters are identified by matching experimental trajectories with simulation results. Then the method of synthesizing the optimal control for lumped parameter systems using adaptive-critic based neural networks is applied. The lumped parameter control is finally mapped back to the spatial dimension, using the same basis functions. This idea of combining POD and adaptive critic technique was proposed in [Padhi]. Experimental results are presented in this paper, which validate the approach.

2. SystemModel and Experimental Setup

2.1 System Model

The diffusion problem is modeled in this study as

$$\frac{\partial x(t,y)}{\partial t} = \alpha(y)\frac{\partial^2 x(t,y)}{\partial y^2} + S(t,y) \qquad (1)$$

where $x(t,y)$ is temperature profile at time $t \in [t_0, t_f]$ and spatial position $y \in [y_0, y_f]$, $\alpha(y)$ is thermal diffusivity and $S(t,y)$ represents overall source (control) term. Since we use distributed control of the thermal diffusion system, we formulate the discrete actuators as follows:

$$S(t,y) = \sum_{m=1}^{M_u} S_m(t,y) \qquad (2)$$

where $S_m(t,y)$ is source term distribution for heater-m and M_u is total number of discrete actuators. We define

$$S_m(t,y) \triangleq \beta(y) q_m(y)\, u_m(t) \qquad (3)$$

where, $\beta(y) \triangleq \alpha(y)/k$ (k being thermal conductivity), $q_m(y)$ is distribution of thermal power source term for heater-m located at $y = y_m$ at full (100%) load and $u_m(t)$ is the control magnitude in

[1] Contact Person, Email: bala@umr.edu, Tel.: 1(573) 341-4675

This research was supported by NSF grant ECS 9976588.

percentage load of heater- m . The boundary conditions (insulated at both ends) are given by $\left[\partial x(t,y)/\partial y\right]_{y_0,y_f} = 0$.

2.2 Experimental Setup

A schematic of the hardware setup to implement the one-dimensional diffusion problem is given in Figure 1 and the actual heat diffusion system is shown in Figure 2. It consists of a series of aluminum slabs and heaters placed one after another. Ten heaters and nine aluminum slabs were assembled. Mica heaters were selected for their small thickness of 0.000635 meters (0.025") of the heating element. The heaters are 0.1524 meters (6") in diameter and have a lead bulge of 0.00508 m (0.2") thick on one of their faces where the leading wires are connected to the heater. Aluminum slabs 0.1524 meters (6") in diameter, and 0.0127 meters (0.5") thick were selected for their high thermal conductivity. A notch was cut on one of the faces of the aluminum slabs to accommodate the lead bulge of the heater. A hole of 0.003175 m (0.125") in diameter was drilled radially into the side of each of the aluminum slabs in order to place a thermocouple within the slab. Since these holes facilitate temperature measurements, they were placed diametrically opposite to the notch to measure the temperature at a point farthest away from lead bulge of two heaters assembled on either sides of the slab. In order to minimize the effect of discontinuity in heat conduction on the temperature measurements due to the presence of the notch, two consecutive slabs were rotated by 90°. K-type thermocouples were used for the temperature measurement; their tips were placed at the bottom of holes 0.0508 m (2") deep.

The software used for input and output of data, namely thermocouple reading and heater control was LabVIEW (installed on a PC with Pentium-I processor). The heaters were connected to 120 volts power supply through Solid State Relays (SSR). The ON and OFF sequence as well as load control of the heaters was possible. In order to control the operating load of the heaters, they were switched ON for a predetermined period of time during each cycle time. During each cycle, the data was written to a digital I/O for predetermined number of times after an interval of thirty-five milliseconds (limited by the SSR specification), updating the status of each of the heaters to ON or OFF depending on the current desired load for each heater. The heater level cycle time N_C is calculated using $N_C = 0.035N_t$, where N_t is number of times data was written to digital I/O during each cycle. The cycle time used in this research is 4.5 Sec.

2.3 Finite Difference Model

A main task of this research was to estimate the system parameters $\alpha(y)$ and $\beta(y)q_m(y)$ before synthesizing the control. Towards this goal, we have used a finite-difference approximation of the system dynamics to propagate its behavior. The Tri-Diagonal Matrix Algorithm (TDMA) [Anderson] was used in this regard. Using a backward finite difference method in Eq.(1-3) and rearranging the resulting equations, the system dynamics can be written as

$$-A_i x_{i+1}^k + B_i x_i^k - C_i x_{i-1}^k = D_i \qquad (4)$$

where k represents the time increment and i represents the spatial increment and the matrices are given by:

$$A_i = \frac{\alpha_i}{\Delta y^2}, \quad B_i = \left[\frac{2\alpha_i}{\Delta y^2} + \frac{1}{\Delta t}\right] \qquad (5a)$$

$$C_i = \frac{\alpha_i}{\Delta y^2}, \quad D_i = \frac{x_i^{k-1}}{\Delta t} + \sum_{m=1}^{M_u} \beta_i (q_m)_i (u_m)_i^k \qquad (5b)$$

The parameters of the numerical simulation using TDMA were selected such that the experimental results were in agreement with the simulation results. For acceptable numerical simulation results the truncation error must be small and the finite difference representation of the marching method needs to meet the conditions of consistency and stability [Anderson]. To keep the size of round-off errors small, it is required that $A_i > 0, B_i > 0, C_i > 0$ and $B_i > A_i + C_i$. These conditions are satisfied our study. For modeling we picked 217 nodes with $\Delta t = 0.01\,Sec$ and $\Delta y = 5.267 \times 10^{-4} m$. These results were simulated at 10 Sec intervals.

2.4 Estimation of System Parameters

2.4.1 Estimation of Thermal Diffusivity: The first step in modeling the system was to arrive at a value of thermal diffusivity $\alpha(y)$, which in our case was assumed to be *constant* over the entire spatial domain. The TDMA simulations were made to match the cooling curve plots of eleven thermocouples by selecting different values of α by trial and error. In our case $\alpha = 0.085\, m^2/Sec$ lead to a very close match between the experimental and simulation results and we selected this value for the control synthesis.

2.4.2 Estimation of Control Effect: Modeling of the control effect was a bit involved. The development has to properly account for the discrete nature of the heater locations. Besides it should be done in such a form so as to make it amenable for the control synthesis and implementation. For this reason, we had to need to find an approximation of the δ function suggested in [Padhi] for incorporating the control effect at discrete spatial locations.

One can notice that the effect of any heater is strongly felt in a small neighborhood of its actual location. In the analytical and experimental studies of thermal processes by [Doumanidis], the heat input by a point source term has been described by a Gaussian power density function. Following this philosophy, we attempted to represent the effect of heater - m at 100% load as $\beta(y)q_m(y)$, where $\beta(y)$ is as defined in Subsection 2.1 and $q_m(y)$ is the distribution function for the source. For any other load less than 100%, we augment this term by a load factor term $0 \le u_m(t) \le 1$ and write the actual effect of control as $\beta(y)q_m(y)\,u_m(t)$. The goal of control design then is to come up with values for $u_m(t)$ for $m = 1,\ldots,M_u$. As a limitation for the actuator used in this experiment, $u_m(t)$ can have only integer values.

For heater - m (located at y_m), we write the source term as a Gaussian distribution function given by

$$\hat{\beta}(y)\hat{q}_m(y) = \frac{k_m}{\sqrt{2\pi}\sigma_m} \exp\left[\frac{-(y-y_m)^2}{2\sigma_m^2}\right] \qquad (6)$$

where k_m is scaling factor, σ_m is standard deviation The parameters of the distribution in Eq.(6) are found by minimizing the cost function:

$$E(k_m, \sigma_m) = \left[\int_{y_0}^{y_f} \beta(y)q_m(y)\,dy - \int_{y_0}^{y_f} \hat{\beta}(y)\hat{q}_m(y)\,dy\right]^2 \qquad (7)$$

We also imposed a constraint that the maximum values of $\beta(y)q_m(y)$ should be matched by the Gaussian model. The system constraint is given by

$$\hat{\beta}_m\hat{q}_m(k_m,\sigma_m,y_m)=\max[\beta(y)q_m(y)] \tag{8}$$

where k_m is the scaling factor and σ_m is the standard deviation for heater-m. To compute an average value of β, we define $\hat{\beta}_m=(\hat{\beta}_m\hat{q}_m(y))_{\max}$ and then derive the following

$$\bar{\hat{q}}_m(y)=\frac{\hat{\beta}_m\hat{q}_m(y)}{(\hat{\beta}_m\hat{q}_m(y))_{\max}}$$
$$\bar{\bar{\beta}}=\frac{1}{M_u}\sum_{m=1}^{M_u}\hat{\beta}_m \tag{9}$$

3. Formulation as a Lumped Parameter Problem

3.1 Problem Definition

The objective of our study was to find an optimal control for the system described by Eq.(1-3). We rewrite these equations as:

$$\frac{\partial x(t,y)}{\partial t}=\alpha\frac{\partial x^2(t,y)}{\partial y^2}+\bar{\bar{\beta}}\,u(t,y) \tag{10}$$

where $$u(t,y)=\sum_{m=1}^{M_u}\bar{\hat{q}}_m(y)v(t,y) \tag{11}$$

The objective is to find an *optimal control* $u(t,y)$, which minimizes the *quadratic cost function:*

$$J=\frac{1}{2}\int_{t_0}^{t_f\to\infty}\int_{y_0}^{y_f}\left[qx^2(t,y)+ru^2(t,y)\right]dydt$$
$$=\frac{1}{2}\int_{t_0}^{t_f\to\infty}\left(q\langle x,x\rangle+r\langle u,u\rangle\right)dt \tag{12}$$

where $q\geq 0, r>0$ are the weights on state and control respectively. Note that there should not be any confusion between the q in Eq.(12) with the q_m in Eq.(3, 7-9), which represent two different quantities.

One can note that even though we introduce a continuous control variable $v(t,y)$ in Eq.(11), the actual control to be implemented $u(t,y)$ still remains discrete. The introduction of continuous control $v(t,y)$ was dictated by our choice of using the continuous basis functions later in Eq.(14). This definition leads to a seemingly different definition of control as defined in Eq.(1-3). However modeling of the system as discussed in Section-2 essentially leads to identification of the system parameters whereas in this section our definition is based on development of a model from a controller synthesis perspective. As parameter identification and modeling for controller synthesis are two different aspects of the system, the above definition of control in Eq.(11) does not lead to any conflict with the definition in Eq.(1-3) from the control implementation point of view.

3.2 Proper Orthogonal Decomposition: Design of Problem-oriented Basis Functions

The main objective for using the POD technique in this study was to find an optimal set of basis functions to span an ensemble of data. Let $\{U_i(y): 1\leq i\leq N,\ y_0\leq y\leq y_f\}$ be a set of N snapshot solutions of the dynamic system. The goal of the POD technique is to design a set of basis functions which has the largest mean square projection on the snapshots. In other words, it was desired to design a function Φ, which maximizes the cost function:

$$I=\frac{1}{N}\sum_{i=1}^{N}\left|\langle U_i,\Phi\rangle\right|^2/\langle\Phi,\Phi\rangle \tag{13}$$

where $\langle\Phi,\Psi\rangle=\int_{y_0}^{y_f}\Phi(y)\Psi(y)\,dy$. The objective is to seek $\Phi=\sum_{i=1}^{N}w_iU_i$, where the coefficients w_i are to be determined such that Φ maximizes I in Eq.(13). In the process we obtain N orthonormal basis functions $\Phi_i, i=1,\ldots,N$. Depending on the energy content, this eigen spectrum is truncated to retain only $\tilde{N}\leq N$ eigen functions for using in the Galerkin projection. An interested reader may see [Ravindran] for a detail discussion on the basis function design procedure.

In this research the experimental data generated for modeling the heaters was treated as snapshots to be used in the POD modeling. As the objective of collecting the snapshots was to develop problem oriented basis functions, which were continuous over the entire spatial domain, spline curve-fits were used to generate data between the consecutive thermocouple readings. Further, the snapshots were collected from the experimental data at equal intervals of time. 572 snap shots (N) were collected, which represented the dimension of the untruncated eigenspectrum. To reduce the order of the system for finding the ($\tilde{N}$) orthonormal eigenfunctions, the ratio $\sum_{j=1}^{\tilde{N}}\lambda_j/\sum_{j=1}^{N}\lambda_j$ was plotted for different values of $\tilde{N}$. It was observed that 99% of the ratio is accounted for by the first three eigenvalues. Hence a third-order model was considered accurate to capture the essential characteristics contained in the snap shots. To validate the previous conclusion, the above procedure of basis function calculations were repeated by doubling the number of snapshots from experimental data by halving the time interval considered earlier. There was, however, no appreciable change and hence the earlier computation was good enough.

3.3 Finite-dimensional Approximation: Galerkin Projection

After obtaining basis functions, we expand $x(t,y)$ and $v(t,y)$ as

$$x(t,y)=\sum_{j=1}^{\tilde{N}}\hat{x}_j(t)\,.\,\Phi_j(y)$$
$$v(t,y)=\sum_{j=1}^{\tilde{N}}\hat{v}_j(t)\,\Phi_j(y) \tag{14}$$

One can notice that we consider the same basis functions for $x(t,y)$ and $v(t,y)$. We assume that the same basis functions are capable of representing the state as well as the control since eventually we aim for a state feedback control. Substituting

Eq.(14) into Eq.(10), taking the inner product with the basis function Φ_j, $j = 1,\ldots,\tilde{N}$ and carrying out some algebra we obtain:

$$\dot{\hat{X}} = A\hat{X} + B\hat{U} \tag{15}$$

where $\hat{X} \equiv [\hat{x}_1, \hat{x}_2, \ldots, \hat{x}_{\tilde{N}}]^T$, $\hat{U} \equiv \begin{bmatrix} \hat{v}_1 & \hat{v}_2 & \cdots & \hat{v}_{\tilde{N}} \end{bmatrix}^T$ and

$$A = \left[a_{ij}\right]_{\tilde{N}\times\tilde{N}}, \quad B = \left[b_{ij}\right]_{\tilde{N}\times\tilde{N}} \tag{16a}$$

$$a_{ij} = -\int_{y_0}^{y_f} \left(\Phi_j'(y).\Phi_i'(y).\alpha(y)\right) dy$$

$$b_{ij} = \bar{\beta} \sum_{m=1}^{M_q} \int_{y_0}^{y_f} \left(\Phi_j(y)\Phi_i(y)\bar{\bar{q}}_m(y)\right) dy \tag{16b}$$

Similarly, after carrying out some algebra [Padhi] we also observe:

$$q\langle x, x\rangle = \hat{X}^T Q\ \hat{X}, \quad r\langle u, u\rangle = \hat{U}^T RU \tag{17}$$

where $Q = diag\begin{pmatrix} q_1 & q_2 & \cdots & q_{\tilde{N}} \end{pmatrix}$, $R = rB$, which enables us to write the cost function in Eq.(13) as

$$J = \frac{1}{2}\int_0^{t_f \to \infty} \left(\hat{X}^T Q\hat{X} + \hat{U}^T R\hat{U}\right) dt \tag{18}$$

4. Adaptive Critic Based Optimal Control Synthesis

4.1 Optimal Control Formulation

The adaptive critic based optimal control synthesis is based on the discrete-time representation of system dynamics and cost function. For this reason, we need to have an analogous optimal control formulation of the lumped system in the discrete time framework. Introducing Δt as the step size in time, we can write:

$$\hat{X}_{k+1} = A_D\, \hat{X}_k + B_D\, \hat{U}_k \tag{19}$$

$$J = \frac{1}{2}\left[\sum_{k=1}^{\infty} \left(\hat{X}_k{}^T Q_D \hat{X}_k + \hat{U}_k{}^T R_D \hat{U}_k\right)\right] \tag{20}$$

where $A_D = I + \Delta t\, A$, $B_D = \Delta t\, B$, $Q_D = \Delta t\, Q$, $R_D = \Delta t\, R$. Following the principle of approximate dynamic programming [Balakrishnan], one arrives at the following optimal control and costate equations respectively on an optimal trajectory.

$$\hat{U}_k^* = -R_D^{-1}\ B_D{}^T \lambda_{k+1} \tag{21}$$

$$\lambda_k = Q_D X_k + A_D{}^T \lambda_{k+1} \tag{22}$$

In the cost function Eq.(18, 20), we used $Q = diag(1\ \ 1\ \ 1)$ and $R = 10^3 diag(1\ \ 1\ \ 1)$. We have used $\Delta t = 0.01$ Sec as the sample time in Eq.(19-22).

4.2 Adaptive-Critic Controller Synthesis

Adaptive-critic optimal control design technique is based on the iterative and mutual training between critic and action neural networks. In this study we use the available experimental snap shots for adaptive critic neural network training, in addition to using these for basis function calculations.

We synthesize critic networks (assuming the action network to be optimal), as follows (Figure 3).

1. Generate a set of $\hat{X}_k$ values. For each $\hat{X}_k$, follow the steps below.
   a. Get $\hat{U}_k$ from the action networks
   b. Get $\hat{X}_{k+1}$ from the *state equation*, Eq.(19)
   c. Input $\hat{X}_{k+1}$ to the trained set of critic network at $(k+1)^{th}$ time step, to get λ_{k+1}
   d. Calculate target critic λ_k^* from *costate equation*, Eq.(22)
2. Train the set of critic networks with input $\hat{X}_k$ and output λ_k^* for the critic network, using all the input-output data together.

We synthesize action networks (assuming the critic network to be optimal), as follows (Figure 4).

1. Generate a set of $\hat{X}_k$ values. For each $\hat{X}_k$, follow the steps below.
   a. Get $\hat{U}_k$ from the action networks
   b. Get $\hat{X}_{k+1}$ from the *state equation*, Eq.(19)
   c. Input $\hat{X}_{k+1}$ to the trained set of critic network at $(k+1)^{th}$ time step, to get λ_{k+1}
   d. Get the target optimal control $\hat{U}_k^*$ from Eq.(21)
2. Train the set of action networks with input $\hat{X}_k$ and output $\hat{U}_k^*$, using all the input-output data together.

Once this process of action synthesis is over, we revert to critic synthesis again. The alternate critic and action network training process is continued till no noticeable change in the output is observed in the outputs in the successive training steps. After that, the action networks represent the optimal relationship between the state and control. For further details, one can refer to [Balakrishnan, Padhi].

4.3 Neural Network Structure

In our current implementation we have used a multi-layer feed forward network of the form $\pi_{3,5,3}$ for the critic training and similar network for the action training. Here, $\pi_{3,5,3}$ denotes a neural network with 3 neurons in the input layer, 5 neurons in the hidden layers and 3 neurons in the output layer. We have taken tangent sigmoid function for all the hidden layers and linear function for the output layer.

5. Experimental Results

5.1 Control Implementation

The action network was implemented online, after training it offline. The error in temperature at each heater location with respect to the desired temperature was used as inputs for the control load calculations. Since no sensors were available at the exact heater locations (except for the end points with Heater-1 and Heater-10), linear interpolation of temperature of two adjacent thermocouple readings was used. Since the thermocouple readings are susceptible to external noise, in order to reduce the effect of

noise the temperatures were sampled at 1000 samples/sec from the first and second channels of digital I/O and were passed thorough a Bessel Filter at a cutoff frequency of 20 hertz using LabVIEW. The median of 80 temperature samples collected was used as the final temperature reading for calculation of control.
Controller implementation at each time step can be carried out as follows.

- Get the temperature readings at time t_k
- Find the error (state) with respect to the desired temperature profile
- Use linear interpolation to get states for all the 217 nodes. This represents $x(t_k, y)$
- Compute $\hat{X}_k$ from $x(t_k, y)$ using the basis functions
- Use $\hat{X}_k$ in the action network to obtain $\hat{U}$
- Get the desired continuous control $v(t, y)$ from $\hat{U}$
- Round $u_m(t)$ to the nearest integer after computing

$$u_m(t) = \left[\int_{y_0}^{y_f} \bar{q}_m(y) v(t,y) dy\right] / \left[\int_{y_0}^{y_f} \bar{q}_m(y) dy\right] \qquad (23)$$

5.2 Results for Control of Temperature Profiles

The desired profile in the current experiment was to drive the system starting from room temperature to 75^0 C, constant temperature profile. The temperature plot is shown in Figure 5 where the final temperature profile in the steady state reaches the desired temperature profile (the desired profile is plotted as '*' at the final time). The corresponding control values are plotted in Figure 6.

It is clear from the results in Figure 5 that the adaptive critic based neurocontroller is successful in driving the system to the desired final temperature profile; the closeness to the desired profiles at the end points, however, is not as good as at the interior regions. This phenomenon was found to occur in every experiment. Similar discrepancies were observed in the control readings too. It can be noted that in Figure 6, the controls at the boundary nodes are not zero in the steady state. The reason for this behavior can be attributed to the physical setup: total insularity at both ends was not physically realizable. This means there is continuous heat dissipation from the system that is not completely accounted for in the controller synthesis. But this heat loss from the system is not negligible compared to the heat flux input to the system. The heat loss being dominant near boundaries prevents any temperature rise in the steady state. One way to achieve better accuracy at the end points is to tighten the insulation. Another way is to account for radiation effects in the mathematical model. One should exercise caution during the estimation of the model parameters to make sure that the assumptions in arriving at the math model are satisfied to the best possible extent.

In order to demonstrate the versatility of the adaptive critic controller, we selected a parabolic profile with the maximum desired temperature at the center of the setup. Figure 7 shows a plot of the history of the temperature readings at the 10 heater locations. The experiment was started from an arbitrary initial profile, where all the thermocouple readings are close to of 35^0 +/- 5^0 C. A plot of the actual control to achieve the desired profile is presented in Figure 8. It is clear that the controller achieved the desired profile in the steady state.

Even though we have presented only representative results, the adaptive critic based controller was successful in achieving several other desired profiles as well, indicating that the feedback optimal control synthesis approach based on the dual network concept is versatile enough to implement in real-life problems.

6. Conclusions

The feasibility of using an adaptive critic based feedback neurocontroller for reaching desired temperature profiles in a thermal diffusion system has been demonstrated. This study has also shown that for thermal systems the POD method of obtain reduced order models for designing controllers actually works in practice. Furthermore, we have demonstrated how to estimate the parameters for a distributed parameter system for use in the design of a control system. Experimental results indicate the potential of POD based models and adaptive critic based neurocontrollers for use in distributed parameter system applications. Although the system used in this study is a linear DPS, there is no linearity assumption in the development of the control synthesis, which implies that the adaptive critic methodology can be used for nonlinear systems as well.

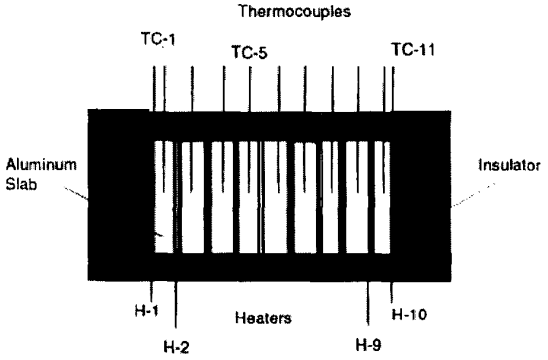

Figure 1: Cross section of experimental setup

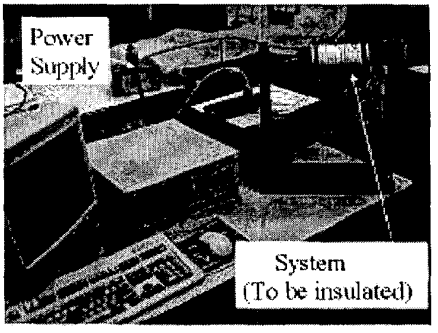

Figure 2: Experimental setup for heat diffusion

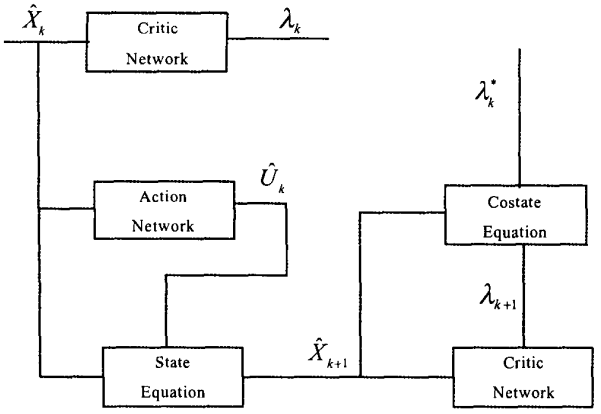

Figure 3: Schematic of critic synthesis

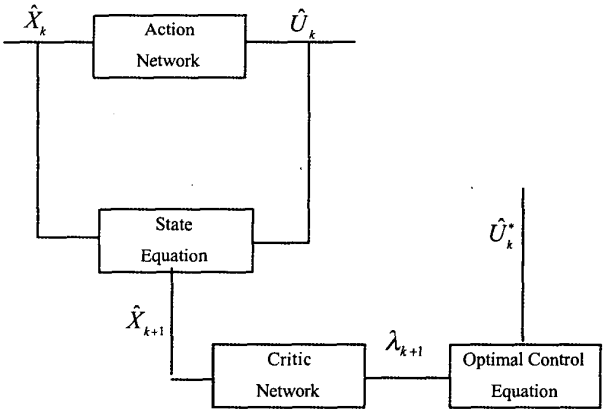

Figure 4: Schematic of action synthesis

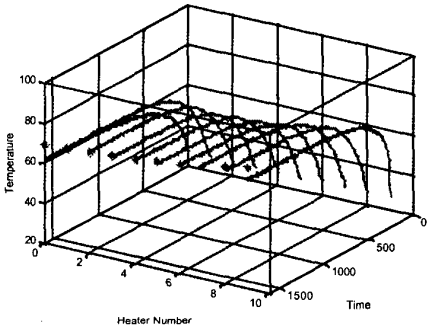

Figure 5: Temperature history for desired parabolic profile

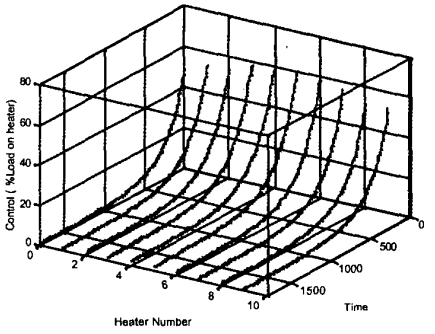

Figure 6: Control load history for Figure 5

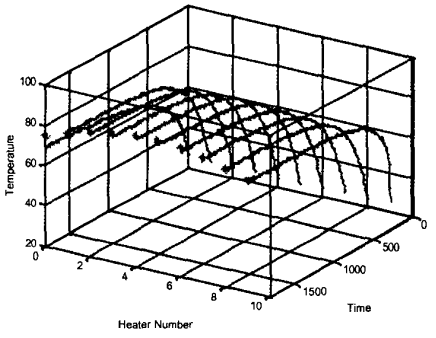

Figure 7: Temperature history for desired parabolic profile

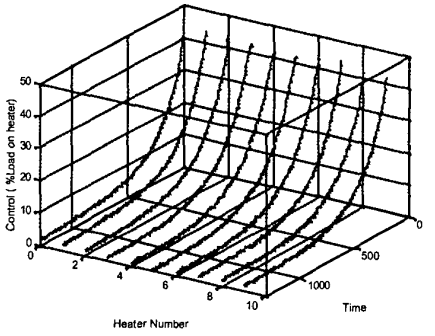

Figure 8: Control load history for Figure 7

References

1. Anderson D. A., Tannehill J. C. and Pletcher R. H., *Computational Fluid Mechanics and Heat Transfer,* Part 1, New York: Hemisphere Publishing Corporation, 1984.
2. Balakrishnan S. N., Biega V., *Adaptive Critic based Neural Networks for Aircraft Optimal Control*, Journal of Guidance, Control and Dynamics, Vol.19, No. 4, pp. 893-898, 1996.
3. Doumanidis C. C. and Fourligkas N., *Temperature Distribution Control in Scanned Thermal Processing of thin Circular Parts*, IEEE Transactions on Control Systems Technology, September, Vol. 9, pp. 708-717, 2001.
4. Padhi R., Balakrishnan S. N., *Proper Orthogonal Decomposition based Optimal Control Design of Heat Equation with Discrete Actuators using Neural Networks*, 15th IFAC World Congress, Paper No. 2735, July, 2002.
5. Ravindran S. S., *Proper Orthogonal Decomposition in Optimal Control of Fluids*, NASA Technical Report, NASA/TM-1999-209113.